HNPS Advances in Nuclear Physics

Vol 32 (2026)

HNPS2025

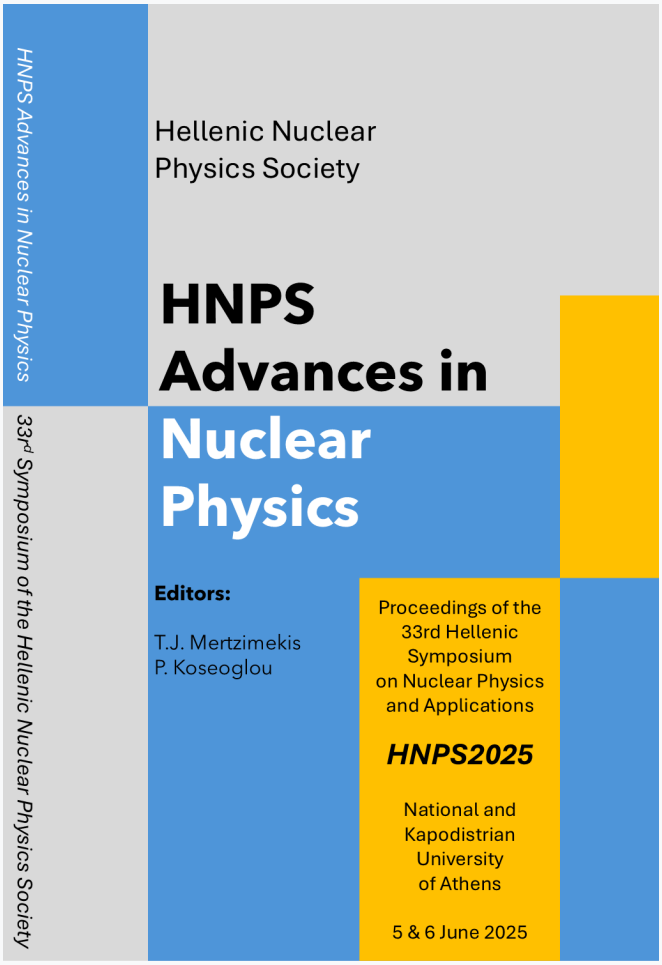

Radio-dating analysis and reconstruction of past events in a semi-closed deep basin, north Cretan Basin

Zoi Maniati, Christos Tsabaris, Effrosyni Androulakaki, Stylianos Alexakis, Dionisis Patiris, K. Manta, Michael Kokkoris

doi: 10.12681/hnpsanp.8838

To cite this article:

Maniati, Z., Tsabaris, C., Androulakaki, E., Alexakis, S., Patiris, D., Manta, K., & Kokkoris, M. (2026). Radio-dating analysis and reconstruction of past events in a semi-closed deep basin, north Cretan Basin. *HNPS Advances in Nuclear Physics*, *32*, 136–143. https://doi.org/10.12681/hnpsanp.8838

HNPS Advances in Nuclear Physics Vol. **32**, 136–143 (2025)
doi: 10.12681/hnpsanp.8838

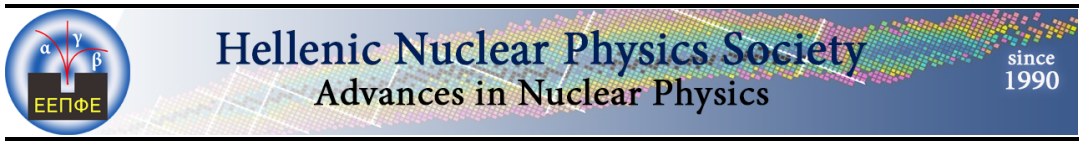

ARTICLE

Radio-dating analysis and reconstruction of past events in a semi-closed deep basin, north Cretan Basin

Z. Maniati,[*,1,2] C. Tsabaris,[1] E.G. Androulakaki,[1] S. Alexakis,[1] D.L. Patiris,[1] K. Manta,[1] and M. Kokkoris[2]

[1]Hellenic Centre for Marine Research, Institute of Oceanography, Anavyssos, Greece
[2]National Technical University of Athens, Department of Physics, Athens, Greece
*Corresponding author: zwhmaniath@gmail.com

(Received: 26 Nov 2025; Accepted: 07 Jan 2026; Published: 14 Jan 2026)

Abstract

The present study investigates recent environmental variations and potential contamination within a semi-enclosed marine basin by examining sediment cores, which serve as both archives and ultimate sinks of particulate and dissolved matter. Sediment samples were retrieved using a box corer and analyzed through high-resolution gamma-ray spectrometry to quantify radionuclide activities and determine bulk density.

The sedimentation rate was derived from the depth distribution of excess ^{210}Pb, with ^{226}Ra used as a supporting radionuclide for equilibrium assessment. A distinct tephra layer identified at 10.5 cm depth was radiometrically dated to approximately 1650 AD, indicating deposition from the Kolumbo volcanic eruption. Notably, the peak activity of natural radionuclides occurs at 9.5 cm, reflecting post-eruptive sedimentary processes.

The lower values of the sedimentation rate observed in this deep basin, compared to the basins of the North and central Aegean Sea, is attributed to its remoteness from direct terrestrial inputs. Furthermore, the relationship between ^{226}Ra and ^{212}Pb delineates two distinct depositional regimes—one preceding and one following the tephra horizon—demonstrating differences in sediment dynamics and related processes.

Keywords: HPGE; gamma-spectrometry; radioactivity; marine environment

1. Introduction

Deep-sea sediments in the Cretan basin act as archives of Mediterranean climate history. The study of chemical and physical magnitudes (such as radionuclides and sediment composition) can reconstruct sea surface temperatures, oxygenation events (sapropel layers through organic-rich deposits), Saharan dust input, and support other activities related to glacial-interglacial cycles and their influence on Mediterranean circulation. As regards the reconstruction processes of the last century in terms of the sedimentological and volcanic history, the Cretan basin recorded volcanic ash layers

 ISBN 2654-007X (print), 2654-0088 (online).

(e.g., from Santorini/Thira, Methana, and Nisyros eruptions) since these events (e.g., tephra accumulation) are chronostratigraphic markers for dating and correlating events. Deep basins also recorded mass-wasting events such as submarine landslides and turbidities, possibly triggered by earthquakes or volcanic activity.

Deep basins in marine environments offer privileged settings for examining long-term changes in sedimentation and the transport of tracers. Due to their relative isolation from terrestrial inputs, the dynamics of material deposition in these regions are principally controlled by deep water circulation [1]. Such conditions make these basins particularly suitable for analyzing sediment layers and reconstructing environmental histories [2].

Radiometric techniques based on measurements of natural and artificial radionuclides are now central to deep-sea sediment studies, acting both as tracers of marine processes and as robust chronological markers. Isotopes including ^{210}Pb and ^{137}Cs enable accurate dating of sediment layers, providing age-depth relationships over the past century [3–5]. These methods help clarify patterns in contaminant input and their comparison with sediment characteristics sheds light on how particles and pollutants are mobilized within the marine system [6].

Recent research has focused on the temporal reconstruction of environmental conditions in deep basins such as those near Lemnos in the North Aegean Sea [7], as well as in other regions like the Adriatic and the Black Sea. Radiochronological analyses were also performed on sediment cores collected from coastal areas of the northeastern Mediterranean Sea [8]. Sediment cores from these environments allow quantitative analysis of radionuclide activities and facilitate the assessment of factors related to climate change and human impact. Age models constructed from ^{210}Pb and validated by ^{137}Cs improve confidence in sedimentation rate estimates and historical reconstructions.

In this work, naturally occurring radionuclides were studied in a sediment core (M3A) from Cretan basin, a semi-enclosed marine area, 25 miles northern from Heraklion port of Crete. Analyzing the distribution of both natural and anthropogenic radionuclides in collected cores has provided new insights into sediment accumulation and material transport with data supporting the application of radiochronological methods previously used in similar basins. Additionally, natural radionuclide profiles and density measurements enable interpretation of sedimentation rates and vertical variations within the study site, highlighting the interplay of environmental and anthropogenic influences over recent centuries.

2. Materials and Methods

2.1 Study area

The coordinates of the sampling point were 35° 43’ 34.68” N, 25° 7’ 50.52” E, which is the M3A station. The sediment core was collected with a box corer sampler from a deep basin of 1500 m. This basin, known as the Cretan Basin, is located within the Cretan Sea, north of Crete.

The South Aegean Basin consists of three principal subregions: the Myrtoan Sea in the northwest, the shallow Cyclades Plateau in the northeast, and the Cretan Sea Basin, which extends across the southernmost part of the Aegean. Among these, the Cretan Sea is distinguished as both the largest and deepest, containing two pronounced troughs in its eastern area that exceed 2400 m in depth, with an average depth of approximately 1000 m. Serving as a reservoir of heat, salinity, and dissolved oxygen, the Cretan basin shows elevated temperature values (above 14°C), salinity levels greater than 38.9 PSU (usual value of East Mediterranean Deep Water is 38.7 PSU [9]), and dissolved oxygen concentration greater than 4.9 ml/l within its intermediate and deep layers [10].

In the northern sector of the study area lies the Kolumbo submarine volcano, situated approximately

7 km northeast of Santorini. This underwater volcanic system was the site of a major eruption in 1650 AD, an event that had profound effects on Santorini and the nearby regions. The eruption released large volumes of volcanic gases, which, upon reaching the atmosphere, proved highly toxic and resulted in the deaths of about 70 people on Santorini [11].

2.2 Sample preparation

Sediment samples were prepared according to the protocols outlined by the IAEA [12]. The 31-cm sediment core was sectioned into 1 cm intervals, which were subsequently dried in an oven at 50°C for 3 days, until their mass stabilized and no further loss of moisture was observed. After drying, each sample was weighed and finely ground using an agate mortar to ensure homogeneity. The powdered samples were then transferred into cylindrical containers, Fig. 1 with dimensions of 6.8 cm in diameter and 1.9 cm in height, and their final masses were recorded. The samples are not fully filled, as variations in density (Fig. 2) result in differences in sediment height. Subsequently, the samples were sealed with paper masking tape Fig. 1 in order to maintain radioactive equilibrium and prevent the escape of gases.

Figure 1. An empty cylindrical container and a sealed container that encloses the powdered sample

2.3 Gamma ray spectrometry measurements

Gamma-ray spectroscopy analyses were performed utilizing a high-purity germanium (HPGe) detector (CANBERRA BE5030, diameter 101.6 mm, length 133.35 mm [13]). Each sample was measured over a 24-h period. To maximize detection efficiency, samples were placed in direct contact with the detector endcap, thereby optimizing the sample-to-crystal solid angle. The spectra of the samples were analyzed with the SPECTRW program [14]. The detector efficiency was determined using a reference IAEA-385 soil source (density 1.2 g/cm^3) [15]. The results were then corrected using the TCS and ET factors, applying the EFFTRAN 4.5 software [16]. The TCS factor accounts for true coincidence summing effects of cascade radionuclides and can reach values up to 1.3 (e.g. ^{214}Bi), while the ET factor compensates for differences in geometry, density and composition between the reference source and the samples or among the samples (e.g. density variations). To calculate the correction factors, it was necessary to create an input file in the EFFTRAN program that describes the geometry of the detector. After the reference source, an inert organic material (talc) with a density of 0.8 g/cm^3 was placed on the detector in the same container as the reference source in order to measure the background radiation.

The specific activity or activity concentration A (Bq/kg) for each radionuclide was calculated using Eq. (1).

$$A = \frac{cps \cdot TCS}{eff \cdot I_\gamma \cdot m} \cdot ET \tag{1}$$

The net count rate (cps), measured in counts/s, for each photopeak was derived from the spectra, while the sample mass (m) expressed in kg, the probability of gamma ray emission (I_γ), the full energy peak efficiency (eff) of the detector and the correction factors (TCS, ET) were also considered in

the calculations. The net counts of the photopeaks are obtained by subtracting the corresponding background counts.

The activity concentration of ^{210}Pb, ^{226}Ra and ^{214}Bi were determined from the counts of the photopeaks at 46 keV, 186 keV, and 609 keV, respectively.

The minimum detectable activity (MDA) was determined from the background spectrum. In the spectrum, the regions of interest (ROI) correspond to the photopeaks at 46 keV, 186 keV, and 609 keV. Eq. (2) was applied to each photopeak using a 95% confidence level:

$$L_D = 2.71 + 3.29\sqrt{B(1 + \frac{N}{2M})} \tag{2}$$

where L_D is the detection limit (in counts), B is the area of background continuum under the peak (in counts), N is the number of channels of the ROI and M is the channels on each side of the peak width. In this study, $M = 5$ was adopted. The background area (B) was determined according to: $B = \frac{(B_1+B_2)N}{2M}$, where B_1 and B_2 are the total counts within the M channels to the left and right of the ROI, respectively.

The MDA (in $Bq \cdot kg^{-1}$) was calculated using the following equation [15]:

$$MDA = \frac{L_D}{eff \cdot I_\gamma \cdot t \cdot m} \tag{3}$$

where eff is the the photopeak efficiency, I_γ is the gamma-ray emission probability, t is the spectrum acquisition time for each sample (in seconds), and m is the mass of the sample (in kg). The MDA uncertainties were propagated from the uncertainties of B_1, B_2, the efficiency and the mass of the samples.

2.4 Dating model

The dating model used in this study is the CF:CS model, which assumes a constant sediment flux and a constant sedimentation rate in the study area [17, 18]. This model was selected due to its assumptions and the specific characteristics of the sampling site. The Cretan Basin is a deep, isolated basin where constant and stable sedimentation is expected, with minimal disturbance from terrestrial sources. According to the CF:CS model, the constant flux denotes the steady influx of excess ^{210}Pb to the sediment surface, while the sedimentation rate was calculated using the radioactive decay law, Eq. (4).

$$A(z) = A_0 \cdot e^{\frac{-\lambda \cdot z}{v}} \rightarrow ln(A) = ln(A_0) - \lambda\frac{z}{v} \tag{4}$$

Where, A is the activity concentration of ^{210}Pb$_{ex}$, z refers to the depth of the sediment core in cm, v is the sedimentation/accumulation rate measured in cm/yr, λ corresponds to the decay constant expressed in yr^{-1}m, and A_0 is the activity concentration of the excess ^{210}Pb for $z = 0$.

The activity concentration of ^{210}Pb$_{ex}$ was calculated as the difference between the total ^{210}Pb activity and the ^{226}Ra activity (^{210}Pb$_{ex}$=^{210}Pb-^{226}Ra). The ^{226}Ra activity concentration was calculated from the 186.2 keV (I_γ=3.5%) peak. This peak is indistinguishable from the ^{235}U peak at 185.7 keV (I_γ=57%). Therefore, the contribution of ^{235}U is properly subtracted. The assumptions made for the calculation are a constant isotopic ratio, ^{238}U (99.3%) ^{235}U (0.7%) and radioactive equilibrium of ^{226}Ra with ^{238}U.

3. Results

The density was calculated from the measured mass of each sample and is shown in Fig. 2. The x-axis represents the density values of the samples (g/cm^3), while the y-axis shows the depth of

the sediment core (cm). Density varies from (0.461±0.003) g/cm^3 at 0.5 cm (surface sediment) to (0.989±.003) g/cm^3 at 10.5 cm. A thin 1-cm layer of black material was observed at 10.5–11.5 cm, which was identified as tephra.

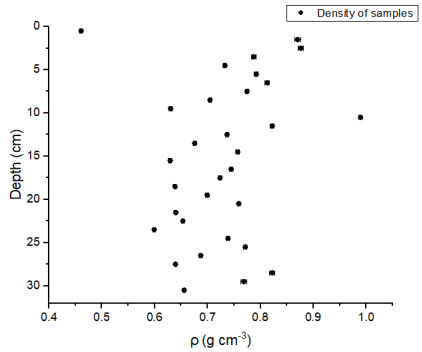

Figure 2. Density of the samples

From calculations using the CF:CS dating model, the sedimentation/accumulation rate is (0.036±0.007) cm/yr. The tephra was dated to 1653 AD (±58 years), assuming a depth of 11 cm and considering the minimum value of the sedimentation rate's 1σ confidence interval, which is 0.03 cm/yr. Therefore, the tephra layer may have originated from the Kolumbo eruption.

The activity concentration of ^{226}Ra ranges from (16±4) to (34±9) Bq/kg, that of ^{214}Bi varies from (15±1) Bq/kg to (31±5) Bq/kg, while for total ^{210}Pb it ranges from MDA to (302±12) Bq/kg, Table 1. Figs. 3a and 3b show the vertical profiles of ^{226}Ra and ^{214}Bi, as functions of the sediment core depth,

Table 1. Table of activity concentration range of ^{226}Ra, ^{214}Bi and ^{210}Pb and MDA values

Energy (keV)	Radionuclides	Activity (Bq/kg)	MDA (Bq/kg)
46	^{210}Pb	MDA - (302±12)	(17.1±0.5)
186	^{226}Ra	(16±4) - (34±9)	(12.0±1.5)
609	^{214}Bi	(15±1) - (31±5)	(6.0±0.3)

along with the dating results from the CF:CS model. The activity concentration of ^{226}Ra increases at a depth of 0.5 cm in the core (34 Bq/kg) and remains constant between 1.5 and 5.5 cm. Then, the activity rises from 6.5 cm, reaching 33 Bq/kg at 8.5 cm, stabilizes for the next 1 cm, and drops again. Between 11.5 and 31.5 cm, the activity remains nearly constant.

The activity of ^{214}Bi starts at 23 Bq/kg, decreases between 1.5 and 4.5 cm, then increases, reaching a maximum of 31 Bq/kg at 9.5 cm. Afterward, the activity drops between 10.5 and 11.5 cm and finally remains constant from 12.5 to 31.5 cm.

Fig. 4a shows the vertical profiles of total and excess ^{210}Pb alongside the dating results. The activity concentrations of ^{210}Pb and ^{210}Pb$_{ex}$ decrease after 4.5 cm, with ^{210}Pb$_{ex}$ approaching zero, as expected.

The calculated MDA values, along with their associated uncertainties, are presented in Table 1 for the radionuclides ^{226}Ra, ^{214}Bi and ^{210}Pb. The variability of MDA with depth primarily reflects differences in sample mass and detector efficiency. Indicative MDA values for the sample taken at a depth of 11.5 cm in the sediment core are reported in the Table.

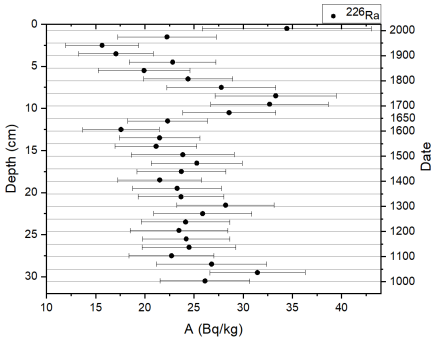

(a) Activity concentration profile of ^{226}Ra

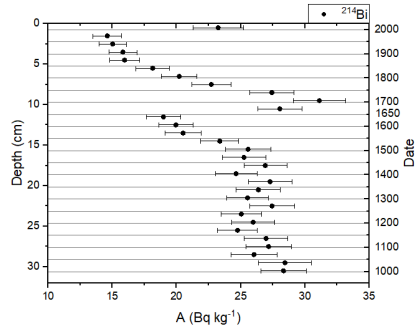

(b) Activity concentration profile of ^{214}Bi

Figure 3

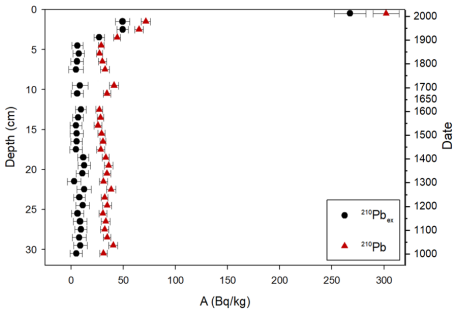

(a) Activity concentration profiles of ^{210}Pb and ^{210}Pb$_{ex}$. In the distribution of ^{210}Pb$_{ex}$ activity concentration, the data points that do not appear are close to the MDA

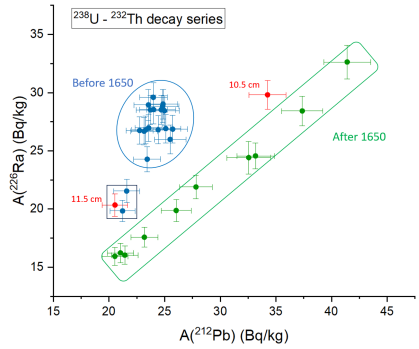

(b) Activity concentration of ^{212}Pb as a function of the ^{226}Ra activity

Figure 4

The activity concentration of ^{226}Ra as a function of ^{212}Pb activity is presented in Fig. 4b, providing insights into the sediment dynamics of the system. Distinct systems can be identified based on variations between ^{226}Ra and ^{212}Pb, with parent isotopes ^{238}U and ^{232}Th, respectively. At depths from 14.5 to 30.5 cm, the Th/U ratio is approximately 24/27.5, which is below unity. Between 11.5 and 13.5 cm depth, the ratio of Th activity to U activity approaches 1, specifically 20.5/20.3 at 11.5 cm. At 10.5 cm (tephra layer), the measured ratio is 34.3/29.8, indicating Th activity exceeds that of U. This condition persists from 0.5 to 9.5 cm, corresponding to to samples dated after 1650 AD. Variations in the Th/U ratios are associated with shifts in sediment composition, suggesting changes in the geochemical characteristics of the material [19]. According to Klaver [20], rocks and pumices from Kolumbo are characterized by elevated Th/U ratios, related to the volcano's regional geology. The graph exhibits a notable difference in Th/U ratios between samples at 10.5 cm and 11.5 cm depths. Overall, the data reveal three distinct systems based on Th/U ratios: one with ratios <1 predating 1650 AD (14.5–30.5 cm), one with ratios near 1 (11.5–13.5 cm), and one with ratios >1 in post-ash samples (0.5–9.5 cm).

4. Summary - Perspectives

In this study, the ^{210}Pb dating model was applied and yielded a sedimentation rate of 0.03 cm/year. Sediment accumulation in the Cretan Basin appears to be slower than that in the deeper basins of

the North and Central Aegean Sea, likely due to the limited terrestrial input to the region. The established chronology of the core provides valuable insights into the distribution of natural radionuclides and the deposition of volcanic tephra.

A tephra layer was visually identified by a distinct color change at 11 cm depth and was dated to approximately 1653 AD, a possible correlation with the Kolumbo volcanic eruption (1650 AD) based on the ^{210}Pb dating model. Ongoing geochemical analyses aim to further characterize the composition of this layer and to clarify the volcanic and post-depositional processes that contributed to its formation. Notably, the highest radionuclide activity concentration was observed at 9.5 cm depth, while the maximum sediment density occurred within the tephra layer. This elevated density may be attributed to the presence of volcanic material within the sediment at that depth.

The application of nuclear analytical techniques enables the identification and interpretation of geological processes/phenomena that have occurred over the past century. Such methods facilitate the reconstruction of historical trends in radioactive contaminants, thereby improving our understanding of their potential effects on marine ecosystems and, indirectly, on human health. Furthermore, using radionuclide activities measured in sediments, seawater concentrations can be estimated through appropriate concentration factors, allowing the assessment of the exposure of marine organisms to both natural and anthropogenic radionuclides within the studied system.

Acknowledgements

This work was supported by the MARRE project through National Strategic Reference Framework (NSRF) 2014–2020 co-financed by Greece and the European Union (European Social Fund ESF). The authors would also want to acknowledge the crew of the research vessel R/V AEGEAO for the sampling using the box corer during the cruise in the frame of MARRE project. The HCMR group would like also to acknowledge IAEA (RER7015 project) due to know-how transfer in terms of reconstruction of environmental magnitudes, as well as the EU Horizon project with the acronym CONTRAST supporting updated tools for interpreting signatures from anthropogenic and natural processes using sediment cores.

Funding statement

This project received funding from the European Union's Horizon Europe programme under the acronym CONTRAST.

References

[1] Georgia Kousidou, Christos Tsabaris, Filothei Pappa, Effrosyni Androulakaki, Gerasimos Korres, and Evangelia Krassakopoulou. "Impact of climate change to sedimentation processes and microplastics gradients: a case study in a semi-closed deep ocean system, Lemnos basin, Greece". In: 31 (2025), 96–101. DOI: 10.12681/hnpsanp.7999.

[2] J. Liu, X. Zhao, N. Chen, Q. Liu, M. Zhang, L. Zhang, R. Novikau, and X. Hou. "The transport, distribution, and budget of anthropogenic 129I in the Bohai and North Yellow Seas, China". In: *Journal of Hazardous Materials* 487 (2025), p. 137101. ISSN: 0304-3894. DOI: 10.1016/j.jhazmat.2025.137101.

[3] A. Ghanem, A. Nada, H. Abozeid, S. Madcour W.and Shetaia, and N. Imam. "Historical trends of heavy metals applying radio-dating and neutron activation analysis (NAA) in sediment cores, Burullus Lagoon, Egypt". In: *Environmental Science and Pollution Research* 31 (June 2024), pp. 43633–43658. DOI: 10.1007/s11356-024-33761-5.

[4] F.K. Pappa, C. Tsabaris, D. Patiris, E. Androulakaki, G. Eleftheriou, C. Betsou, V. Michalopoulou, M. Kokkoris, and R. Vlastou. "Historical trends and assessment of radionuclides and heavy metals in sediments near an abandoned mine, Lavrio, Greece". In: *Environmental Science and Pollution Research* 25 (Oct. 2018), pp. 1–17. DOI: 10.1007/s11356-018-2984-0.

[5] F.K. Pappa, C. Tsabaris, D.L. Patiris, E.G. Androulakaki, A. Ioannidou, G. Eleftheriou, M. Kokkoris, and R. Vlastou. "Dispersion pattern of 226Ra and 235U using the ERICA Tool in the coastal mining area, Ierissos Gulf, Greece". In: *Applied Radiation and Isotopes* 145 (2019), pp. 198–204. ISSN: 0969-8043. DOI: 10.1016/j.apradiso.2018.12.021.

[6] A. Vinković et al. "Could atmospheric carbon be driving sedimentation?" In: *Journal of Soils and Sediments* 22 (July 2022). DOI: 10.1007/s11368-022-03282-0.

[7] C. Tsabaris, G. Kousidou, E. Androulakaki, D. Patiris, F.K. Pappa, D. Marmara, and E. Krasakopoulou. "Reconstruction of radioactivity and microplastic particles studying sedimentation/accumulation in the deep Lemnos basin, North Aegean Sea, Greece". In: *Journal of Soils and Sediments* 24 (Sept. 2024), pp. 3938–3952. DOI: 10.1007/s11368-024-03907-6.

[8] G. Eleftheriou, C. Tsabaris, D. Papageorgiou, D. Patiris, E.G. Androulakaki, and F.K. Pappa. "Radiometric dating of sediment cores from aquatic environments of north-east Mediterranean". In: *Journal of Radioanalytical and Nuclear Chemistry* 316 (Mar. 2018). DOI: 10.1007/s10967-018-5802-8.

[9] S. E. Poulos. "Water Masses of the Mediterranean Sea and Black Sea: An Overview". In: *Water (Switzerland)* 15.18 (2023). Cited by: 12; All Open Access, Gold Open Access, Green Open Access. DOI: 10.3390/w15183194.

[10] D. Kassis, E. Krasakopoulou, G. Korres, G. Petihakis, and G. Triantafyllou. "Hydrodynamic features of the South Aegean Sea as derived from Argo T/S and dissolved oxygen profiles in the area". In: *Ocean Dynamics* 66 (Sept. 2016). DOI: 10.1007/s10236-016-0987-2.

[11] F. Fouque and A. R. McBirney. "Santorini and its eruptions". In: 1998. URL: https://api.semanticscholar.org/CorpusID:127842208.

[12] U. Barnekow, S. Fesenko, V. Kashparov, G. Kis-Benedek, G. Matisoff, Yu. Onda, N. Sanzharova, S. Tarjan, A. Tyler, and B. Varga. *Guidelines on Soil and Vegetation Sampling for Radiological Monitoring, Technical Reports Series No. 486.* Tech. rep. International Atomic Energy Agency, 2019.

[13] E. Georgali and ... et al. "Characterization of the Canberra BE5030 Broad Energy High Purity Germanium Detector by means of the GEANT4 Monte Carlo simulation package". In: *HNPS Advances in Nuclear Physics* 27 (2020), 152–154. DOI: 10.12681/hnps.3002.

[14] C.A. Kalfas, M. Axiotis, and C. Tsabaris. "SPECTRW: A software package for nuclear and atomic spectroscopy". In: *Nuclear Instruments and Methods in Physics Research Section A: Accelerators, Spectrometers, Detectors and Associated Equipment* 830 (2016), pp. 265–274. ISSN: 0168-9002. DOI: 10.1016/j.nima.2016.05.098.

[15] G. Eleftheriou, C. Tsabaris, E.G. Androulakaki, F.K. Pappa, and D.L. Patiris. "High resolution gamma-ray spectrometry for routine measurements of environmental samples". In: *Applied Radiation and Isotopes* 206 (2024), p. 111234. ISSN: 0969-8043. DOI: 10.1016/j.apradiso.2024.111234.

[16] Tim Vidmar. "EFFTRAN—A Monte Carlo efficiency transfer code for gamma-ray spectrometry". In: *Nuclear Instruments and Methods in Physics Research Section A: Accelerators, Spectrometers, Detectors and Associated Equipment* 550.3 (2005), pp. 603–608. ISSN: 0168-9002. DOI: 10.1016/j.nima.2005.05.055.

[17] F.K. Pappa, C. Tsabaris, D. Patiris, E. Androulakaki, G. Eleftheriou, C. Betsou, V. Michalopoulou, M. Kokkoris, and R. Vlastou. "Historical trends and assessment of radionuclides and heavy metals in sediments near an abandoned mine, Lavrio, Greece". In: *Environmental Science and Pollution Research* 25 (Oct. 2018), pp. 1–17. DOI: 10.1007/s11356-018-2984-0.

[18] J.A. Sanchez-Cabeza and A.C. Ruiz-Fernández. "210Pb sediment radiochronology: An integrated formulation and classification of dating models". In: *Geochimica et Cosmochimica Acta* 82 (2012). Environmental Records of Anthropogenic Impacts, pp. 183–200. ISSN: 0016-7037. DOI: 10.1016/j.gca.2010.12.024.

[19] Zhi-jun Dai, Jinzhou Du, Ao Chu, and Xiao-Ling Zhang. "Sediment characteristics in the North Branch of the Yangtze Estuary based on radioisotope tracers". In: *Environmental Earth Sciences - ENVIRON EARTH SCI* 62 (Apr. 2011), pp. 1629–1634. DOI: 10.1007/s12665-010-0647-7.

[20] M. Klaver, S. Carey, P. Nomikou, I. Smet, A. Godelitsas, and P.Z. Vroon. "A distinct source and differentiation history for Kolumbo submarine volcano, Santorini volcanic field, Aegean arc". In: *Geochemistry, Geophysics, Geosystems* 17 (July 2016). DOI: 10.1002/2016GC006398.